

Experimental investigations from conventional to high speed milling on a 304L stainless steel.

A. Maurel-Pantel^{*1}, M. Fontaine², G. Michel², S. Thibaud², J.C. Gelin²

¹*LMA, Aix-Marseille Univ, CNRS, UPR 7051, Centrale Marseille, F-13402 Marseille Cedex 20, France*

²*FEMTO-ST Institute, Department of Applied Mechanics, UMR CNRS 6174, ENSMM/ UFC / UTBM, France.*

*Corresponding author: Dr. Ing. Aurélien MAUREL-PANTEL

Tel: + 33 (0)4 91 16 42 27

Fax: + 33 (0) 4 91 16 44 81

Email: maurel@lma.cnrs-mrs.fr

Abstract

Last years analytical or finite element models of milling become more efficient and focus on more physical aspects, nevertheless the milling process is still experimentally unknown on a wide range of use. This paper propose to analyse with accuracy milling operations by investigating the cutting forces values, shape of cutting forces curves obtained for different cutting speeds, and related phenomena as tool wear or tool run-out. These detailed experimental data in milling constitute a suitable experimental basis available to develop predictive machining modelling. All the tests have been conducted on the 304L stainless steel in many cutting configurations and for different tool geometries. The machinability of the 304L stainless steel with different tools geometries and configurations in shoulder milling is defined by three working zones: a conventional zone permitting stable cutting (low cutting speed; under 200-250 m.min⁻¹), a dead zone (unfavourable for cutting forces level and cutting stability; between 250 and 450 m.min⁻¹), and a high speed machining zone (high cutting speed; up to 450-500 m.min⁻¹). All the used criteria (cutting forces, chips, wear) confirm the existence of these different zones and a correlation is proposed with cutting perturbations as run-out, cutting instability, ploughing and abrasive wear.

Keywords: *Machinability, High-speed milling, Cutting forces, Tool run-out, 304L stainless steel.*

Nomenclature

ρ	Density
c	Calorific capacity
T	Temperature
β	Taylor-Quinney coefficient
$\bar{\sigma}$	Equivalent stress
$\dot{\bar{\epsilon}}$	Equivalent strain rate
A	Yield stress constant of Johnson-Cook law
B	Strain hardening constant of Johnson-Cook law
n	Strain hardening exponent of Johnson-Cook law
C	Strain rate hardening constant of Johnson-Cook law
m	Temperature dependant coefficient of Johnson-Cook law
$\bar{\epsilon}^p$	Cumulated plastic strain
μ_s	Static friction coefficient
f	Feed rate
N	Spindle frequency
V_C	Cutting speed
f_t	Feed per tooth
d_a	Axial depth of cut
d_r	Radial depth of cut
r_ϵ	Cutting edge radius
ϕ	Tool nominal diameter
τ	Number of elements in the chip maximal section
θ	Angular position of the mill
F_x	Cutting force along the X axis (here Transverse force)
F_y	Cutting force along the Y axis (here Feed force)
F_z	Cutting force along the tool Z axis (here Axial force)

1 Introduction

Milling is one of the most frequently used machining processes in mechanical industries. But some essential physical phenomena are still difficult to understand. Indeed milling is a very complex process with physical interactions between shearing, compression, ploughing, friction, high strain rate, thermal effects, failure and forced vibrations. Nevertheless manufacturing industries own a good empirical knowledge of the process and search essentially to optimise productivity. Although, in academic research field, works on machining focus mainly on turning process and try to extrapolate issues to the milling process.

Many empirical, analytical or finite element models have been developed in orthogonal cutting, in oblique cutting or more recently in 3D turning and 3D milling. At the beginning, Merchant [1] has proposed the first basic analytical model in orthogonal cutting taking into account only shearing effects in a specific plane orthogonal to the cutting edge. Then, Oxley [2] has improved the model with introduction of semi empirical relations and a behaviour law for the machined material. More recently, Ceretti et al. [3] have proposed a finite element model of a 2D orthogonal cutting to reproduce the chip formation with different cutting conditions. Then Baker [4] proposed a finite element model in orthogonal cutting and validate the cutting predictions with experimental cutting forces confrontation. The first milling models were developed with an empirical description of local cutting process based on cutting coefficients, and by using an axial decomposition of the mill to consider elementary straight edges in oblique cutting position by [5] and improved after by Yellowley [6]. Many models based on the same approach were proposed during the twenty following years with some remarkable advances on ball-end milling by Yang and Park [7], in milling process dynamics by Altintas and Lee [8], in an advanced cutters geometrical description by Engin and Altintas [9-10], or even free-form machining by Zhu et al. [11]. But very few more complete models of milling were proposed more complete including specifically an accurate description of different tool geometries, of tool complex pathes and engagement, and taking into consideration the tool run-out. Only one model mixed these developments with a thermo-mechanical description of local cutting process with the purpose to enhance the understanding of milling cutting process, Fontaine et al. [12] validate strong hypotheses associated to oblique cutting and propose a more predictive approach. This model uses the shear band model developed for high speed machining by Molinari et al. [13] and

Dudzinski et al. [14] and the analytical modelling of the 3D oblique cutting configuration developed by Moufki et al. [15]. And now Zeroudi et al. [16] have integrated in model the use of CAM tool paths and Zeroudi and Fontaine [17] have also predicted the produced form and roughness. More recently finite elements models have been extended to milling process but only few detailed experimental research are available in literature : Shao et al. [18] proposed a machinability study on 3%Co-12%Cr stainless steel in milling and D'Errico et al. [19] studied the tool-life reliability of cermet inserts with milling tests. In the FEMTO-ST Institute, a 3D finite element model of milling has been developed with the commercial software LS-Dyna by Maurel-Pantel et al. [20]. This milling simulation is able to model the chip formation, to predict the cutting forces curves and to furnish thermo-mechanical information during the cutting process.

Some experimental research have been also conducted to determine the machinability of the material. Tekiner et al. [21] have developed measurement methods to compare process sound with the cutting parameters in turning of AISI 304 austenitic stainless steel. Sullivan et al. [22] have proposed the on-line work hardening detection techniques to study the machinability of SS303 austenitic stainless steel. Salak et al. [23] have proposed an experimental method to compare the machinability of different powder metallurgy steels in face turning configuration. Other experimental research have been conducted to analyse some different aspects in stainless steel machining as tool wear in order to predict the tool life like in the works of Senthil Kumar et al. [24] or in order to compare free cutting additives influences on cutting conditions as in Akasawa et al. [25], or to study the surface integrity of machined workpiece as in Shao et al. [18], to identify and develop modelling of friction conditions as in Valiorgue et al. [26-27]

and improve numerical model predictivity in turning simulation as in Bonnet et al. [28].

Last years analytical or finite element models of milling become more efficient and focus on more physical aspects, nevertheless the milling process is still experimentally unknown on a wide range of use in literature. Now, it seems interesting to improve the predictive capacity of these models on a wide machining range. Milling experiments in many conditions are necessary to analyse, to understand and to quantify the experimental phenomena with for example the help of cutting forces measurement directly during milling operations.

The works related in the present paper describe a set of milling tests lead on a common stainless steel (AISI 304L). The aim consist to analyse the material behaviour in a wide range of machining conditions, from low speed to high speed machining, in order to obtain a wide experimental knowledge of the machinability of this steel in milling. In this work, the analysis essentially leans on the direct measure of cutting forces during the milling operations and examination of the classical machining results (chips, wear, surface integrity...). The final aim consists to build an accurate experimental basis to develop and improve analytical and finite element models of milling on a wide range of use.

2 The 304L stainless steel

The 304L stainless steel is widely used in product manufacturing because it presents a very good forming capacity, an excellent resistance to corrosion and a high ductility. In last years, use of AISI 304L was widely expanded to other fields as chemical, biomedical and power plant industries. The steel grade 304

represents today 80 % of the world-wide stainless steel market but austenitic stainless steels are usually considered as quite difficult to machine. Actually stainless steel are commonly machined with a maximal cutting speed equal to 250 m.min⁻¹ but this limit increases continually with improvements in machine-tools and tools design. The machinability of this steel is more difficult than other alloy steels due to low heat conductivity, high built-up edge tendency and high deformation hardening. The 304L stainless steel has a face centred cubic structure, and it is composed of purely austenitic phases but a mechanical sollicitation creates carbide and martensite α' . The chemical composition of the material used for experiments is related in Table 1.

Table .1. Chemical composition of the machined 304L stainless steel.

% C	% Si	% Mn	% P	% S	% Cr	% Mo	% Ni	% Ti	% Cu	% Co	% N
0.028	0.26	1.5	0.033	0.03	18.25	-	8.25	-	0.53	0.14	0.0895

Table .2. Material parameters associated to the Johnson-Cook law defined for the 304L stainless steel.

$A(MPa)$	$B(MPa)$	n	C	m	$\dot{\epsilon}_0(s^{-1})$	$T_f(^{\circ}K)$	$T_0(^{\circ}K)$
220	900	0.397	0.0274	0.319	1.0	1698	296

Table .3. Material parameters associated to the modified Merchant law for the 304L stainless steel.

A_1	A_2	λ_f
0.543	0.751	0.65

In results exposed in the paper obtained with analytical model, the material behaviour is described with a Johnson and Cook constitutive law (1) (Johnson and Cook, 1983) [29] and a modified Merchant law [1]. The parameters related in Table 2 and Table 3 are identified with an inverse method based on an objective function build with the measured and numerical cutting forces [30-31].

$$R = [A + B\varepsilon^n] \left[1 + C \ln \left(\frac{\dot{\varepsilon}}{\dot{\varepsilon}_0} \right) \right] \left[1 - \left(\frac{T - T_0}{T_f - T_0} \right)^m \right] \quad (1)$$

Where A corresponds to yield strength, B and n corresponds to the hardening coefficients, C defined the strain rate sensitivity, and m defined the temperature dependency coefficient. T_f and T_0 are respectively the melting temperature and the ambient temperature.

$$\phi = A_1 + A_2(\alpha_n - \lambda_f) \text{ with } \lambda_f = \text{Arctan}(\mu_f) \quad (2)$$

Where λ_f and μ_f are respectively the average friction angle and friction coefficient at the tool/chip interface, α_n corresponds to the normal rake angle defined by the tool geometry and local direction of cutting velocity. A_1 and A_2 parameters depending of the machined material.

3 Milling experiments protocol

3.1 Micro-milling machine

All the milling tests described in this paper were performed at ENSMM (Engineering School in Mechanics and Microtechnics) in Besançon, on a three axes KERN© HSPC2525 micro-milling machine. This machine allows reaching high cutting speeds (spindle frequency up to 35000 rev/min) and guaranties very good repeatability and stability of the tests due to its high rigidity (concrete polymer frame) and high precision (+/- 0.5 μm positioning).

3.2 Cutting forces measurement setup

The cutting forces measurement is performed with a Kistler dynamometer 9272. Classically this product is used in drilling, but it presents a good polyvalence and especially a high frequency bandwidth. The 4 sensors of the device deliver an electric signal proportional to the loads in X, Y and Z directions and the cutting force on each axis are obtained by summation. The dynamometer is connected to a PC through a 5070 Kistler charge amplifier and a National Instruments input/output data acquisition card (sample frequency limit: 40 kHz). Then data is treated through a specific software, in which the sample frequency available is adjustable and always corresponds to an integer multiple of the tooth path frequency. The main device characteristics are exposed in Table 4.

Table 4. Characteristics of the Dynamometer Kistler 9272.

Components	Acquisition range	Frequency limits	precision
F_x, F_y	-5...5 kN or -500...500 N	3.1 kHz	0.5 N
F_z	-5...20 kN or -500...2000 N	6.3 kHz	0.5 N
M_z	-200...200 N.m or -20...20 N.m	4.2 kHz	1 N.m

3.3 Sample geometry

The samples in 304L stainless steel have been machined with a wire EDM process from extruded and hyperquenched bars furnished by Thyssen France. The samples length was chosen in order to have the centre of the tool path in a stabilised machining zone (geometry and setting are exposed on Figure 1). The sample is fixed on the dynamometer through an aluminium part in order to fix properly the sample and to reduce the weight to keep the frequency range. With these cautions and checking good positioning, the solicitations on sensors are balanced and a good operating is assured.

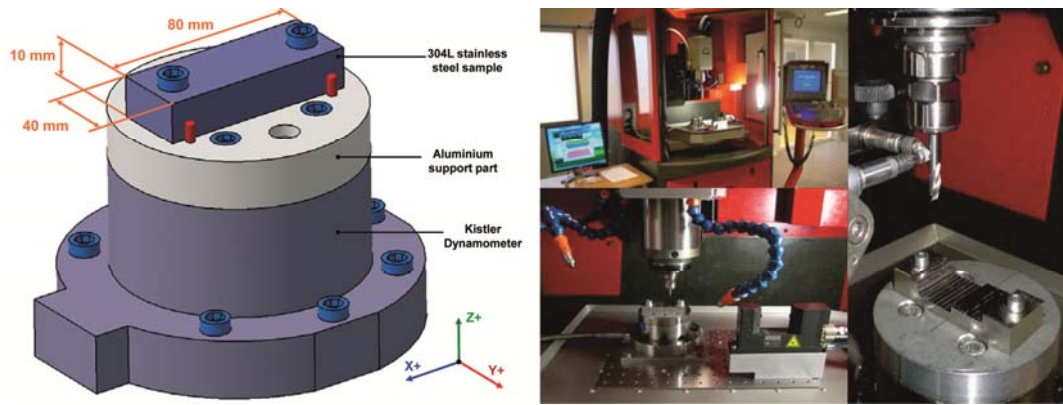


Fig .1. Assembly of the samples used for the experiments and pictures of the milling acquisition systems.

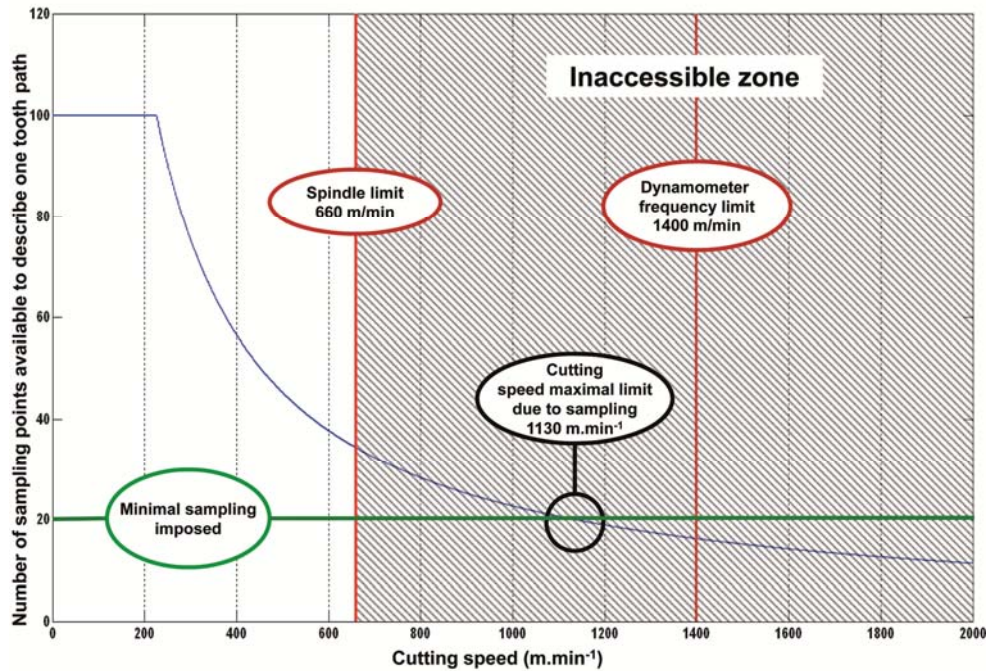


Fig .2. Measure validity range with a 6 mm diameter mill function of cutting speed

3.4 Acquisition limits in milling

The validity range of the cutting forces measurements is described by the cutting speed range available with our acquisition system. Figure 2 exposes the experimental system limits but also describe the actual technological difficulties to reach high cutting speed in milling. The case of a milling operation with a 6 mm diameter end mill is considered accordingly to the experiments.

Figure 2 relates the maximum number of sample points available to describe a tooth path and underlines the technological limits of the experimental setup.

- The first limit consists to keep at minimum 20 sample points by tooth to obtain a good description of the cutting forces curves. This first condition determined by the maximal frequency of the acquisition card, limit the experimental range to a maximal cutting speed of 1130 m.min⁻¹.
- Then, two technological limits appear: the acquisition frequency maximal limit of the dynamometer and the limit of the machine spindle. It is very important to perform the tests below the frequency limit of the dynamometer, that's why we pay attention in our experimental test to keep a gap of 30 % in order to avoid measurement errors due to amplification. The machine spindle impose the more severe criterion in this configuration and the maximal cutting speed reachable experimentally is 660 m.min⁻¹.

3.5 Device used for the analysis

A topo-microscope Alicona has been used for qualitative and quantitative analyses of machined samples. This device is designed to perform optical measures without contact in three dimensions. It is based on an optical microscope coupling with a camera. Topo-microscopy is combination of two types of measure: microscopy and micro-topography. It is possible from obtained high resolution juxtaposed 3D fields to perform measure of dimensions, topography, waviness profile, roughness, surfaces and volumes.

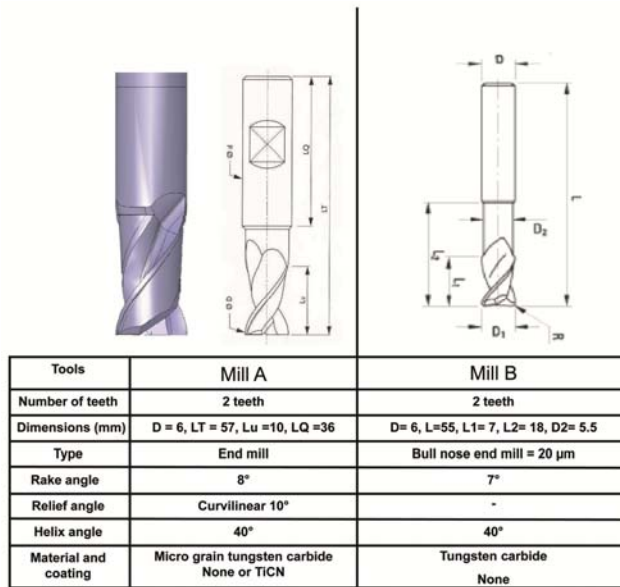


Fig .3. Characteristics of tools used in the experiments.

3.6 Tested tools

In this study, tools are solid cutters made in tungsten carbide coated or uncoated. The mills have been specifically chosen for their good dynamic balancing and good symmetry of cutting edges. The both aspects permit to respect the tool engagement induced by the feed, to avoid the amplification of the radial tool run-out and to reduce vibration phenomena induced by a high spindle frequency. All mills used in experiments have a 6 mm diameter and two teeth in order to simplify the interpretation of cutting forces curves in function of the tool engagement in matter. At the beginning, tests have been led on with coated and uncoated end mills commercially proposed for such applications. The uncoated ones present the benefits to homogenize and simplify the experimental observations. Then, bull nose end mills have been tested for their robustness and to reach higher feed values. The cylindrical end mills (noted mill A) and the bull nose end mills (noted mill B) have been provided by two different manufacturers. The mills characteristics are described and exposed in Figure 3.

Tools	Type	Coating	Cutting speed(m.min ⁻¹)	Feed (mm.tooth ⁻¹)	Configurations
Tool 1	Mill A	-	70 to 650	0.03	Slotting
	Mill A	-	70 to 650	0.015	Up cutting
	Mill A	-	70 to 650	0.03	Up cutting
	Mill A	-	70 to 650	0.045	Up cutting
	Mill A	-	70 to 370	0.06	Up cutting
	Mill A	-	70 to 650	0.03	Down cutting
Tool 2	Mill A	TiCN	70 to 650	0.015	Up cutting
	Mill A	TiCN	70 to 650	0.03	Up cutting
	Mill A	TiCN	70 to 650	0.045	Up cutting
	Mill A	TiCN	70 to 650	0.03	Down cutting
Tool 3	Mill B	-	70 to 590	0.03	Slotting
	Mill B	-	70 to 590	0.01	Up cutting
	Mill B	-	70 to 590	0.015	Up cutting
	Mill B	-	70 to 590	0.03	Up cutting
	Mill B	-	70 to 590	0.045	Up cutting
	Mill B	-	70 to 590	0.06	Up cutting
	Mill B	-	70 to 590	0.015	Down cutting
	Mill B	-	70 to 590	0.03	Down cutting
	Mill B	-	70 to 590	0.045	Down cutting

Table .5. Milling tests performed.

3.7 Tested cutting conditions

Different feeds and cutting configurations, and a large range of cutting speeds were tested with the selected tools. The reference values of cutting speed and feed recommended by tools manufacturers were about 150 m.min⁻¹ and 0.03 mm.tooth⁻¹ respectively. The minimum and maximum values were defined after preliminary milling tests in association with the tool manufacturers. The cutting speed of 650m.min⁻¹ corresponds to the maximum value reachable with a 6 mm diameter mill and the used spindle. All the parameters configurations were tested with a cutting speed pitch of 30 m.min⁻¹ in order to obtain a complete and pertinent data

about machinability of the tested 304L steel. All tested parameters are summed up in Table 5. All tests have been performed in slotting or shoulder milling in down and up cutting configurations. In all milling tests the tool engagement is defined with an axial depth of cut of $d_a = 1$ mm and the radial depth of cut of $d_r = 3$ mm (semi immersion) for the shoulder milling tests.

4 Analysis of milling experiments

All machining tests were led on with micro-lubrication in order to limit difficulties to control and to repeat the cooling conditions. Moreover, lubrication could add a complexity in modelling of the interface between tool and material. This difficulty would be taken into account in numerical models developed, and could add incertitude in models predictivity. Finally, some cutting conditions show that machining stainless steels without lubricant can be efficient and it is interesting to investigate this more earth and health friendly configuration.

All the cutting forces curves measured for milling operations have the characteristic shape exposed on Figure 4. An unstable zone appears at the beginning and at the end of the acquisition. These zones correspond to entry and exit of the tool in sample. In the centre of acquisition curves appears a steady zone that is defined as reference for the different analyses. The vertical milling machine frame (X, Y, Z) is defined as reference for the cutting forces for all figures and discussions. The positive sense on these axes corresponds to the tool displacement in relation to the workpiece in accordance with conventions in machining. As a convention, all forces are considered like acting on the tool and the following legend is always respected in the paper:

- The blue colour is used for transversal forces F_x .

- The red colour is used for feed forces F_y .
- The green colour is used for vertical forces F_z .

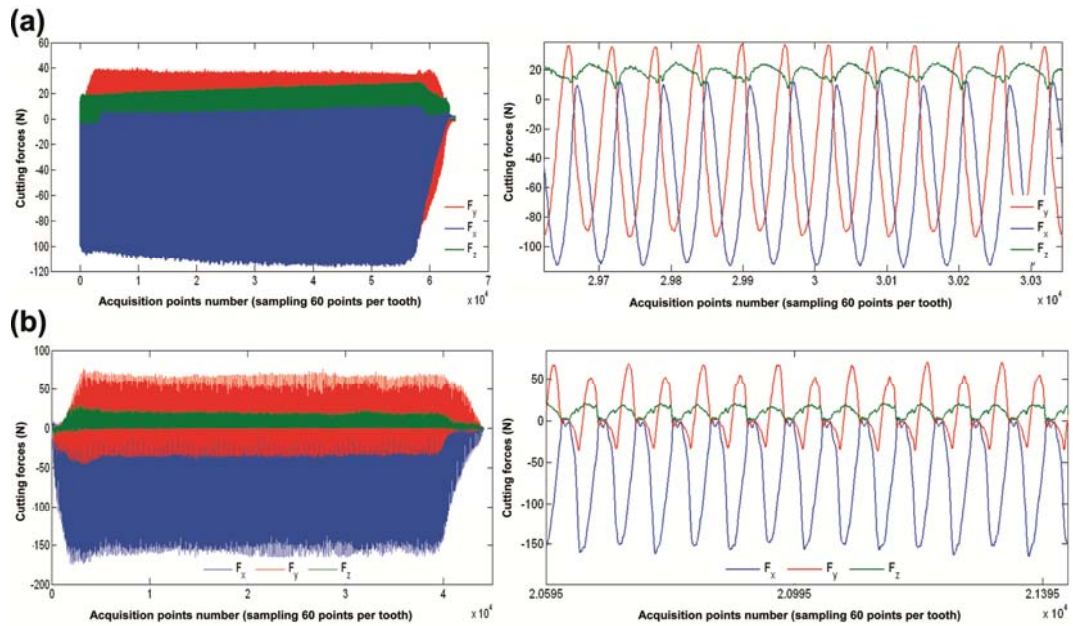


Fig. 4. Measured cutting forces curves with a zoom on the steady zone. (a) slotting configuration and (b) down cutting configuration (semi immersion)

4.1 Cutting configurations in milling

In this section, the main tool engagement conditions in three axes milling are analysed from the cutting forces curves measured and calculated with our analytical model using a rigid description of the tool engagement and firstly proposed in Fontaine et al. [12] [32]. Discussions in this section focus mainly on the transverse force F_x and feed force F_y . Indeed, it is difficult to confront the vertical force F_z with the tool engagement because F_z force it shows lesser cutting force levels and is directly perturbed by non shearing cutting phenomena as ploughing mainly due to the cutting zone at tool end where cutting speed and chip thickness tend to zero. For instance Fontaine et al. [32] described in slotting a confrontation between the negative values on F_z obtained with an end mill and the positive values obtained with a bull nose end mill for which the projection of

local forces on the tool change and the non shearing phenomena at tool end increase. The case considered corresponds to a mill with two teeth, but conclusions can be easily generalised for a mill designed with one, three or more teeth. A spectral analysis has been conducted on each test in order to verify that measures are not disturbed by unexpected frequencies. We are able with this protocol to have a good correlation and interpretation of cutting forces curves with the tool engagement in matter.

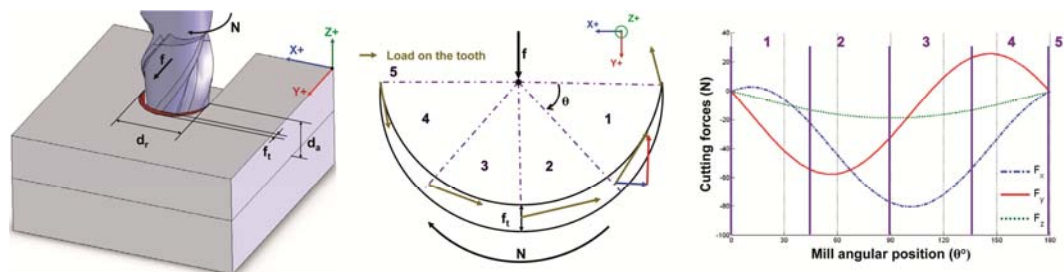


Fig .5. Theoretical tool engagement, tooth path, and cutting forces curves characteristics in slotting configuration

4.1.1 Slotting configuration

In slotting configuration, the radial depth of cut corresponds to the mill diameter ($d_r = 6$ mm). Classically, d_a corresponds to the vertical depth of cut, the configuration is described in Figure 5. If a cross section in (X, Y) plane for an altitude z is considered, the tooth path related in Figure 5 corresponds to the section of material removed by a tooth on a height d_a and a maximum width corresponds to the feed f_t . The mill has a helix angle and the cutting edge follows this helix, that's why the cutting edge is not in the same place for different altitudes z considered. The tool engagement is totally three-dimensional with a trochoidal geometry and imposes the chip motion and formation. These essential remarks put in evidence limits to make comparisons between turning process and

milling process. It is proposed here to analyse cutting forces curves in slotting milling conditions with the assumptions of a rigid tool. The cutting forces curves for a tooth path obtained analytically are related in Figure 5 and the numbers used to locate the extremity of the mill cutting edge along the track in the matter are reported on the cutting forces graphic. The main steps during each tooth path are described in order to understand the curve shapes of a milling operation in slotting configuration. So, five stages are considered. Each one put in evidence a characteristic evolution of the cutting forces curve in the rigid case:

- The stage 1 corresponds to the entrance of the tooth in matter, and in slotting configuration it begins with a chip thickness close to 0 mm. On cutting forces curves, F_y becomes negative when F_x becomes positive and come back quickly to negative values. This phenomenon is due to projection of the forces on the relief face of the tool in contact with the machined surface, and this is characteristic to the tool entrance in matter.
- The stage 2 is the critical place for the feed force F_y . Indeed this step is characterised by the maximal negative value on F_y and a decrease to negative values on F_x .
- The stage 3 corresponds to the maximal loading zone, in this zone the tooth removes a maximal thickness of matter equal to the feed f_t , and the deformed volume of material is maximal. This step is characterised by the maximal negative value on transverse force F_x and by the annulment of the feed force F_y . The stage 3 is the critical place for the force F_x . Usually, this step corresponds also to the maximal value of the vertical force F_z .

- The stage 4 is symmetric to the stage 2. This step is characterised by the maximal positive value on F_y and a force F_x tending to zero.
- The virtual stage 5 corresponds to the outgoing of the tooth in matter. Both forces F_y and F_x are close to zero corresponding to the end of the cutting cycle for the first tooth. In case of slotting with a two teeth end mill, the curves begin immediately another identical cycle with the second tooth as related in Figure 6 (a).

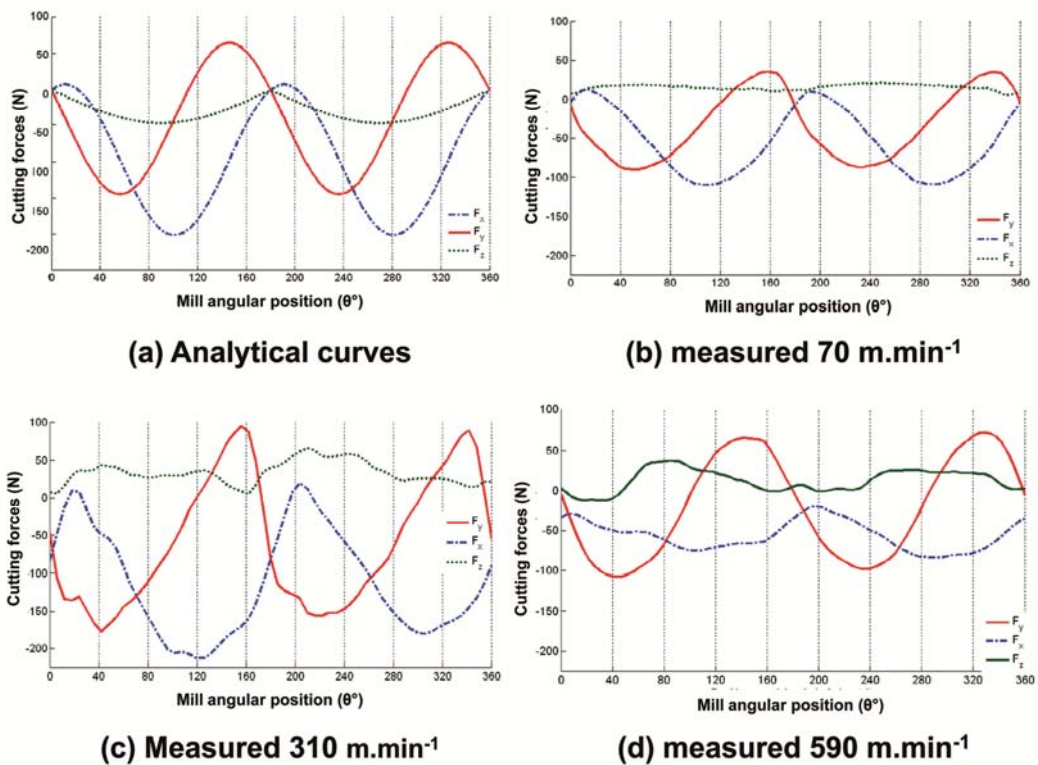


Fig .6. Qualitative comparison of cutting forces curves in slotting configuration with mill A. (a) rigid case obtained analytically. (b) cutting speed equal to 70 m.min⁻¹. (c) cutting speed equal to 310 m.min⁻¹. (d) cutting speed equal to 590 m.min⁻¹. ($f_t = 0.015$ mm.tooth⁻¹, $d_r = 6$ mm, $d_a = 1$ mm)

An angular difference appears between the tool position located and the different stages on the curves. This is due to the fact that the maximal loads are located on a point in the median immersion plane of the mill, and it depends on the depth of cut d_a and the value of the helix angle. The tooth angular position is considered at the extremity of the tool cutting edge and this choice induced the angular

difference observed on the curves. For a mill with more than two teeth, the interpretation would not be easy but the same tendencies will be observed on the resultant force on the tool. This analysis allows having a better understanding to analyse the experimental curves. Figure 6 exposes four sets of cutting forces curves for a mill rotation (two tooth paths in this case). The first cutting forces curves noted (a) are calculated analytically with the material parameters previously exposed and with the same cutting conditions than the cutting forces curves (b) that is to say for a low cutting speed. Cutting forces curves (c) and (d) are chosen respectively for a middle cutting speed and for the higher cutting speed tested in slotting. The curve shapes obtained analytically in a rigid case are equivalent for the three cutting speeds and only the forces level slightly decreases. The best correlation is obtained for the cutting forces curves (b) with the lower cutting speed. In slotting configuration, the tool motion is balanced by the guiding of the slot, and the tool globally respects a motion close to the rigid case considered in machining models. Only some medium cutting speeds imply cutting instabilities and then cutting forces amplification, for example for $310 \text{ m}\cdot\text{min}^{-1}$.

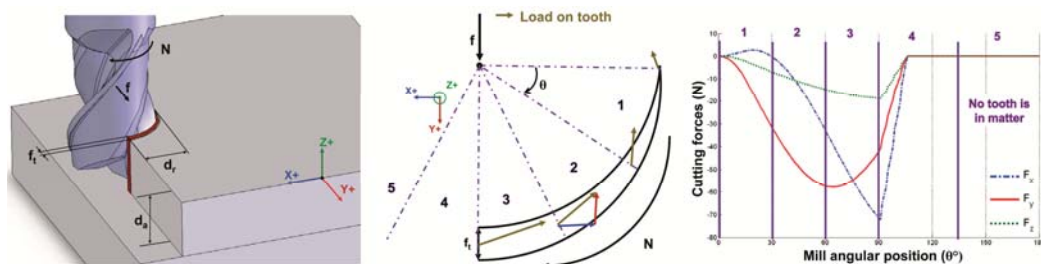


Fig .7. Tool engagement, tooth path, cutting forces curves characteristics in up cutting configuration.

4.1.2 Shoulder milling in up cutting configuration

In up cutting configurations in shoulder milling, the radial depth of cut is strictly inferior to the mill diameter ($d_r < \phi$). The operation is a contouring one and consists to remove the matter only on a side of the tool with an axial depth of cut

d_a . Up cutting configuration is described on figure 7 and corresponds to the case where the matter comes on a mill tooth globally in the opposite way than the tool displacement in relation to the workpiece. The teeth begin to remove matter with a thickness equal to 0 mm and finish cutting with a varying thickness (maximal in case of radial semi-immersion and equal to feed per tooth f_t). The shoulder milling case in up cutting is considered in this paper for a radial semi-immersion (i.e. $d_r = \frac{\phi}{2}$). If a cross section in (X, Y) plane is considered as previously, the tooth path related in Figure 7 corresponds to the section of matter removed by a tooth. Figure 7 described the cutting forces curves obtained in up cutting configuration analytically in a rigid case and like previously the four main stages are described:

- The stage 1 corresponds to the entrance of the tooth in matter, and in this case begins by a thickness equal to 0 mm. For this step same interpretations than in slotting configurations can be considered.
- The stage 2 is the critical place for the feed force like in slotting configuration.
- One more time the stage 3 corresponds to the maximal loading zone. In this position the tooth removes a maximal thickness of material equal to the feed f_t (only in case of semi-immersion). The stage 3 is the critical place for the transverse force F_x and the split-up of the chip. Just after this stage, the chip is removed, and the tooth comes outside the matter, a nickpoint appears on curves, the cutting forces increase quickly to value zero. In this zone the chip separation mode and the tool geometry have a high influence. And lots of phenomena (wear, vibrations...) are initiated in this zone due to the fast change of loading on the tool.

- The stage 4 is characterised by the annullment of the three cutting forces. In this step no tooth is not in contact with matter and the three cutting forces are equal to 0 as related in Figure 7.

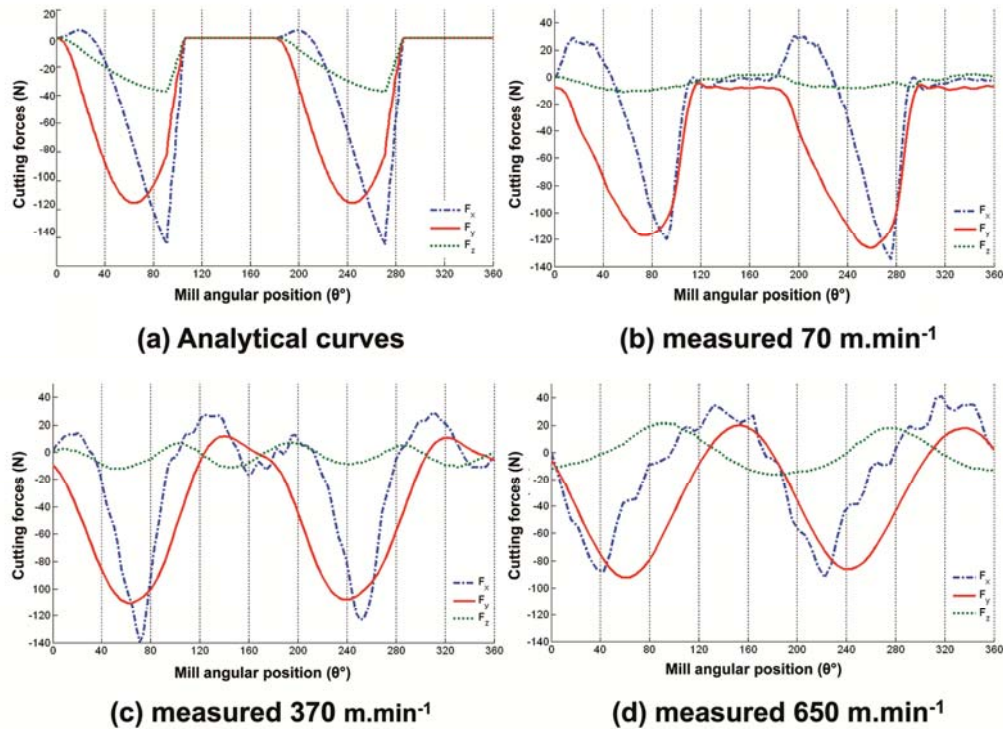


Fig .8. Qualitative comparison of cutting forces curves in shouldering configuration (up cutting) with mill A. (a) rigid case obtained analytically. (b) cutting speed equal to 70 m.min^{-1} . (c) cutting speed equal to 370 m.min^{-1} . (d) cutting speed equal to 650 m.min^{-1} . ($f_t = 0.03 \text{ mm.tooth}^{-1}$, $d_r = 3 \text{ mm}$, $d_a = 1 \text{ mm}$).

For a mill with more than two teeth, the interpretation would not be easy but the same tendencies will be observed on the resultant force on the tool. It is interesting to compare the cutting forces curves of shoulder milling in up cutting configurations for three position cutting speeds with the analytically calculated curves. Figure 8 describe four sets of cutting forces curves, (a) and (b) corresponding to the same milling operations at low cutting speed, (c) corresponding to higher cutting speeds and (d) to high speed machining zone. The cutting forces curves (b) describe the same curves shape than described previously. There is a good correlation for low cutting speed with the assumption of an undeformable tool classically used in machining models. In this case between 0 and 180 m.min^{-1} ,

analytical modelling gives a good description of cutting forces. For higher cutting speeds, some stages disappear. For instance on chart (c) there is no continuous zero value and on (d) the nickpoint has disappeared, the curves are sinusoidal and the cutting process seems to be continuous. Cutting forces curves (d) seems to present the same curve shapes than in slotting operations. Actually, rigid machining models are not able to be predictive in this machining zone. Vibrations phenomena and flexible behaviour of the tool have to be considered in modelling in order to reach high speed milling zones.

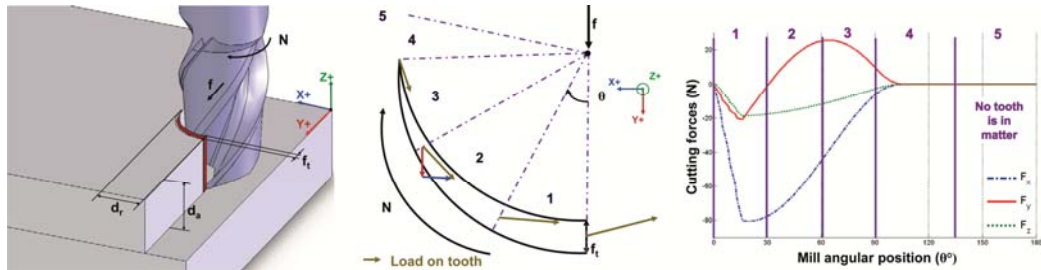


Fig.9. Tool engagement, tooth path, cutting forces curves characteristics in down cutting configuration.

4.1.3 Shoulder milling in down cutting configuration

In down cutting configurations in shoulder milling, the radial depth of cut is strictly inferior to the mill diameter ($d_r < \phi$). The operation is the symmetric of up cutting. Down cutting configuration corresponds to the case where the matter comes on a mill tooth globally in the same way than the tool displacement in relation to the workpiece. The teeth begin to remove matter with a maximal thickness (equal to f_t in semi-immersion case) and finish cutting with thickness equal to 0 mm. This configuration is described in Figure 9. The shoulder milling case in down cutting is considered in this paper for a radial semi-immersion (i.e. $d_r = \frac{\phi}{2}$). If a cross section in (X, Y) plane is considered as previously, the tooth path related in Figure 9 corresponds to the section of material removed by a tooth.

Figure 9 described the cutting forces curves obtained in down cutting configuration analytically in a rigid case and the four main stages can be described:

- The stage 1 corresponds to the tooth entrance in matter, and it begins by a maximal thickness equal to f_t in radial semi-immersion. It corresponds to the maximal loading zone. Nickpoints are observed on three cutting forces curves corresponding to the fast entrance in matter and to the particular form of the first undeformed chips because of the presence of the straight initial workpiece surface. This step are characterised classically by a maximal negative value on transverse force F_x and a decrease of feed force F_y . This negative value of feed force is mainly due to the projection of forces on the tool relief surface and induced by the tool/matter interface. This step is the critical place for the transverse force F_x . The stage 2 corresponds to the feed force F_y annulment and to the beginning of the F_x force decrease.
- The stage 3 is characterised by the maximal positive value on feed force F_y , it is the critical place for the feed force F_y .
- The stage 4 is characterised by the annulment of the three cutting forces. In this step no tooth is in contact with matter.

As previously, Figure 10 describes four sets of cutting forces curves in down cutting configuration. There is a good correlation for low cutting speeds with the assumption of an undeformable tool. Between 0 and 230 m.min⁻¹ in this case, the analytical model predict well the cutting forces. Between 0 and 230 m.min⁻¹ in this case, the analytical model predict well the cutting forces.

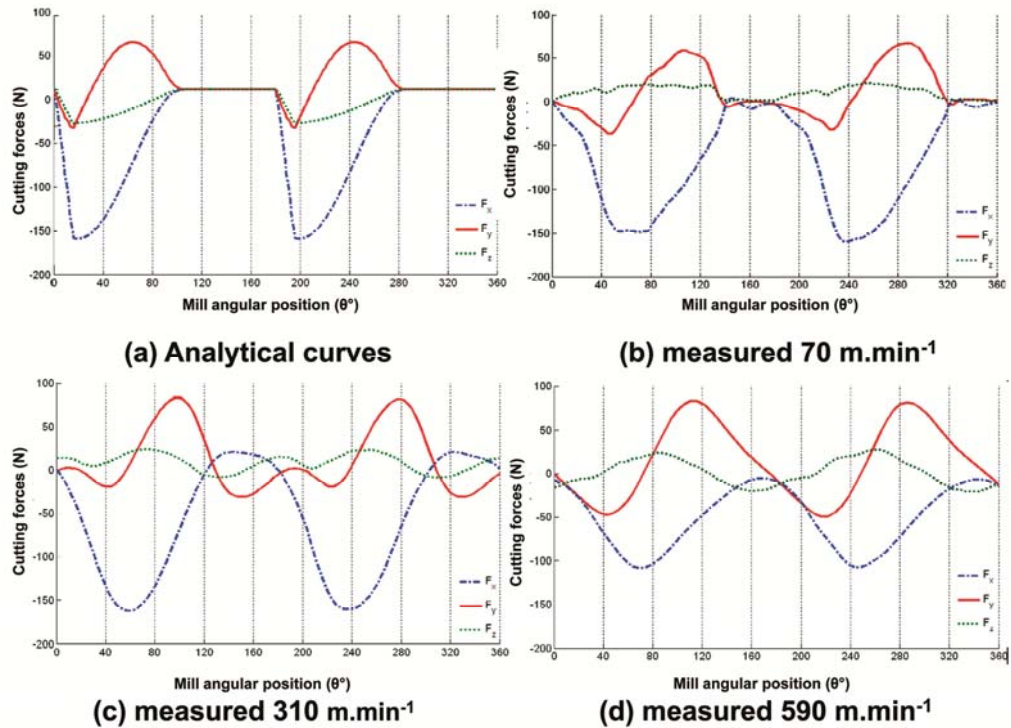


Fig.10. Qualitative comparison of cutting forces curves in shouldering configuration (down milling) with mill B. (a) rigid case obtained analytically. (b) cutting speed equal to 70 m.min⁻¹. (c) cutting speed equal to 310 m.min⁻¹. (d) cutting speed equal to 590 m.min⁻¹. (ft=0.045mm.tooth⁻¹, dr= 3 mm, da= 1 mm).

Between 0 and 230 m.min⁻¹ in this case, the analytical model predict well the cutting forces. For higher cutting speeds, some stages are disappeared. For instance on chart (c) there is no continuous zero value and on (d) the nickpoint has disappeared, the curves are sinusoidal and the cutting process seems to be continuous. For instance on chart (c) there is no continuous zero value and the nickpoint has disappeared. On chart (d) the curves become sinusoidal and the cutting process seems to be continuous. Then there is still a lack in modelling about tool dynamic behaviour and ploughing effects. Complementary experimental investigations as chips, tool wear and cutting forces curves observation with considering tool run-out permit to enhance this description of the cutting phenomena in different machining zones. The aim consists in describing clearly the milling process and putting in evidence process difficulties or specificities. All experiments presented below have been led on in shoulder

milling with up and down cutting configurations (semi radial immersion $d_r = 3$ mm) and with a constant axial depth of cut ($d_a = 1$ mm).

4.2 Machinability of the 304L stainless steel

This analysis focus on the machinability of 304L stainless steel and its behaviour for different tools and in a wide range of cutting speeds. The main criterion is the influence of tools and cutting conditions on the measured cutting forces. In the following section, the average peak-to-peak amplitude values of transverse forces F_x and feed forces F_y are identified in the stabilised zone and are related in function of cutting speed and feed tested in different cutting configurations as shown in Figure 4.

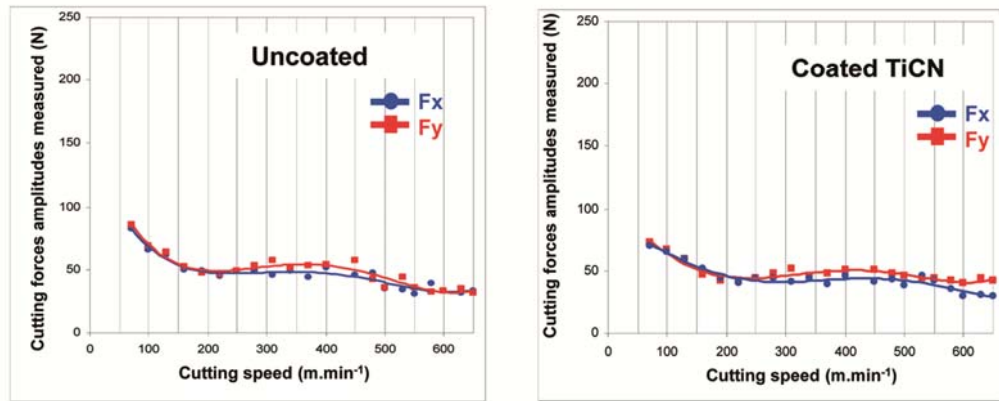
4.2.1 Results obtained with mill A

In the experiments with the end mill A, analysis focus on differences observed between coated and uncoated end mills as related in Figure 11, and following conclusions appeared:

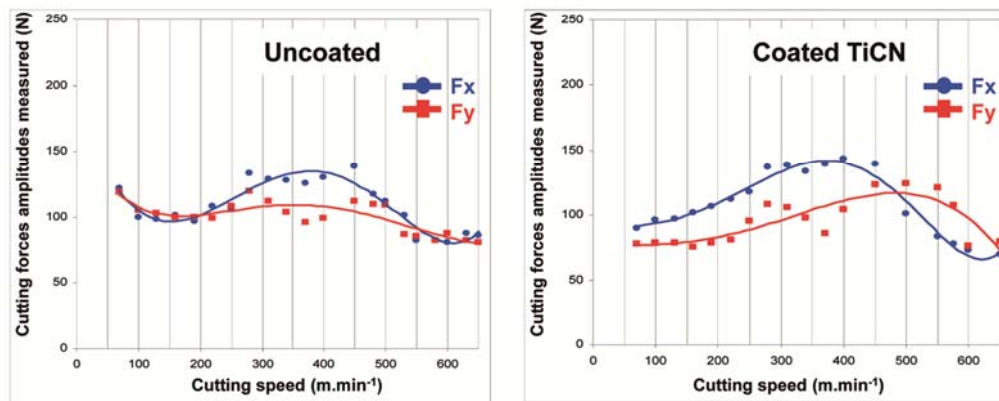
- In both cases (coated and uncoated mill), cutting forces values increase globally proportionally to the feed.
- For the two tools machinability curves are similar, but a difference has to be noted, particularly for high feed values: the levels of cutting forces for the coated mills are appeared slightly lower than for the uncoated ones. The TiN based coatings are well known to significantly reduce the friction at the tool-material interface [33] and it is particularly sensitive in this case because of high load associated to high feed rate and of the sticking behaviour of stainless steels in machining [34].

- On all curves, three working zones are observed: a first zone for small cutting speeds where cutting forces are constant or presenting a light decrease; then a critical second zone where the cutting forces increase strongly appears; and finally a third zone with high cutting speeds where cutting forces decrease strongly and reach values lower than in first zone.
- On all curves, the secondary zone is less favourable and is more critical for high feed values.

$$f_t = 0.015 \text{ mm.tooth}^{-1}$$



$$f_t = 0.03 \text{ mm.tooth}^{-1}$$



$$f_t = 0.045 \text{ mm.tooth}^{-1}$$

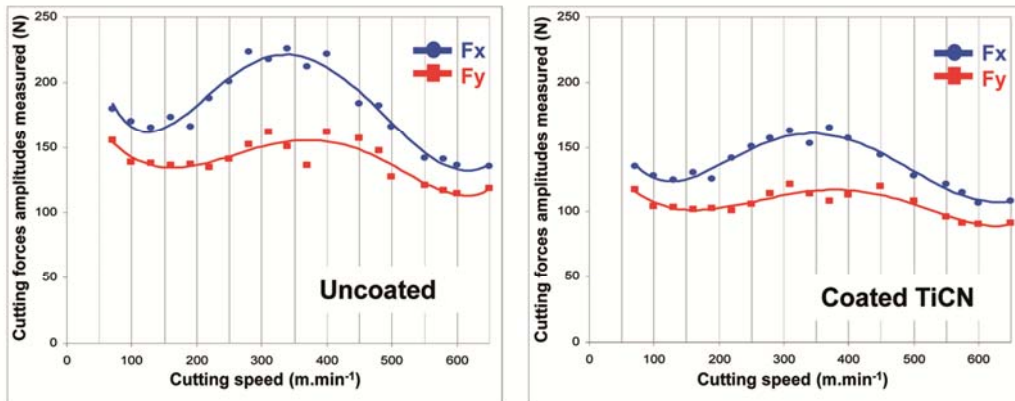


Fig.11. Cutting forces average amplitude evolutions function of cutting speed in up cutting configuration for coated and uncoated end mills A.

4.2.2 Results obtained with mill B

The results obtained with the bull nose end mill B are here analysed. In this case, the both configurations in shoulder milling have been tested and compared. The

curves are related in function of cutting speeds and feeds in up cutting in Figure 12 and in down cutting in Figure 13. The following conclusions appeared:

- Classically and as seen before, in both cases cutting forces values increase proportionally to the feed. But for the both highest feeds, difference is not significant.
- As seen before and in both cases, criticality of the secondary zone directly depends on feed value.
- In down cutting configuration, the lower feeds seem to be unfavourable for the tool, because the cutting forces in first zone reach the same values than for the maximal feeds.
- On these curves, three working zones are observed: a first zone with quite low cutting forces; a critical second zone where these forces increase strongly; and a third zone with high cutting speeds where cutting forces decrease rapidly. In both cases the critical zone has not been observed for the transverse forces F_x . The critical zone exists for the feed forces F_y only in up cutting configuration. Transverse forces describe in second machining zone a stable zone slightly decreasing. This effect is probably due to the bull nose end mill geometry that gives a better resistance to high loading on teeth. With bull nose end mill the critical machining zone is not a problem for the transverse forces F_x .

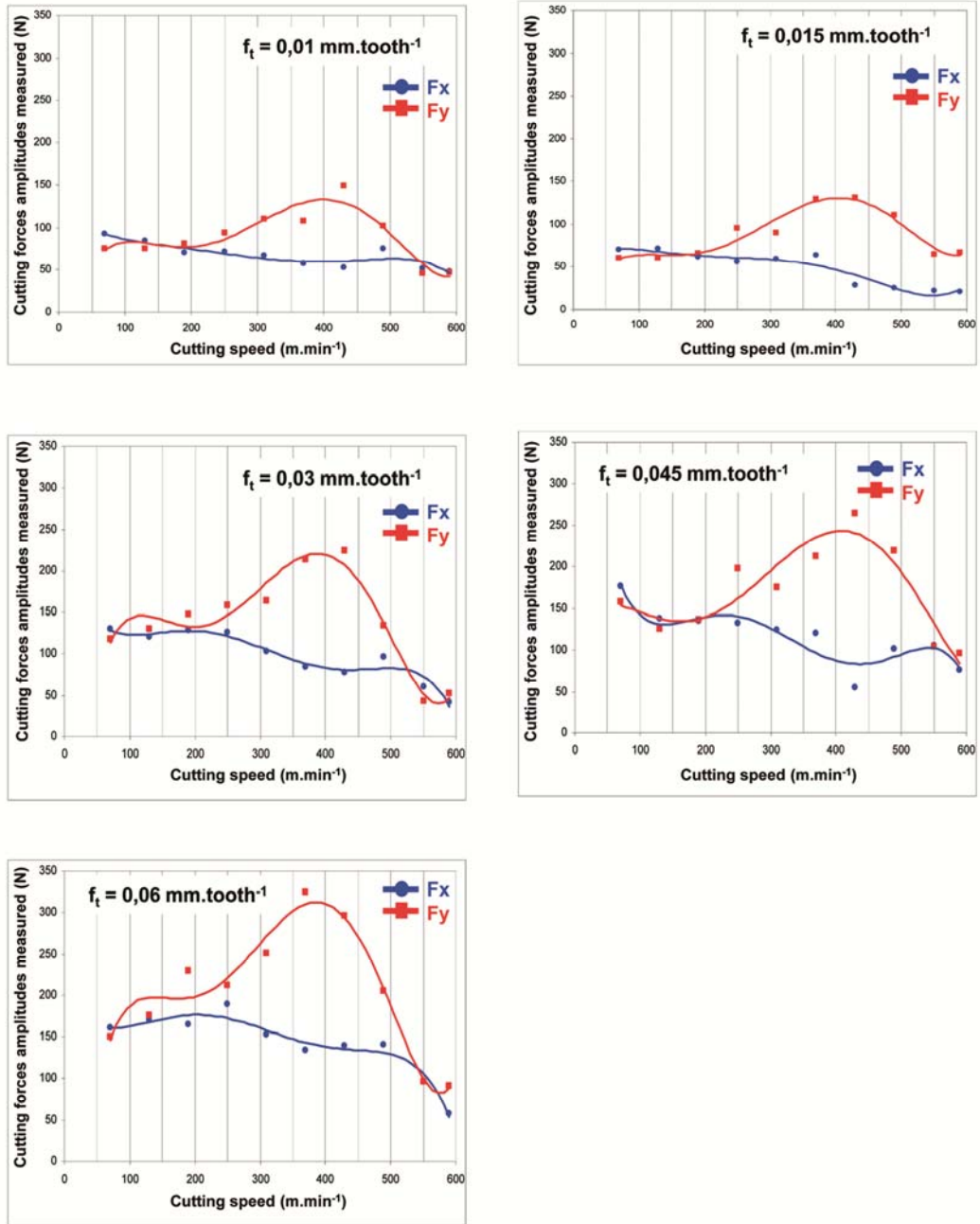


Fig.12. Cutting forces average amplitude evolutions function of cutting speed in up cutting configuration for end mills B.

- In down cutting, the critical zone becomes a stable zone with values equivalent to the first and third zones. This machining zone is not as critical as in the other cases. The shoulder milling in down cutting configuration has showed the best behaviour on the tested cutting speeds range.

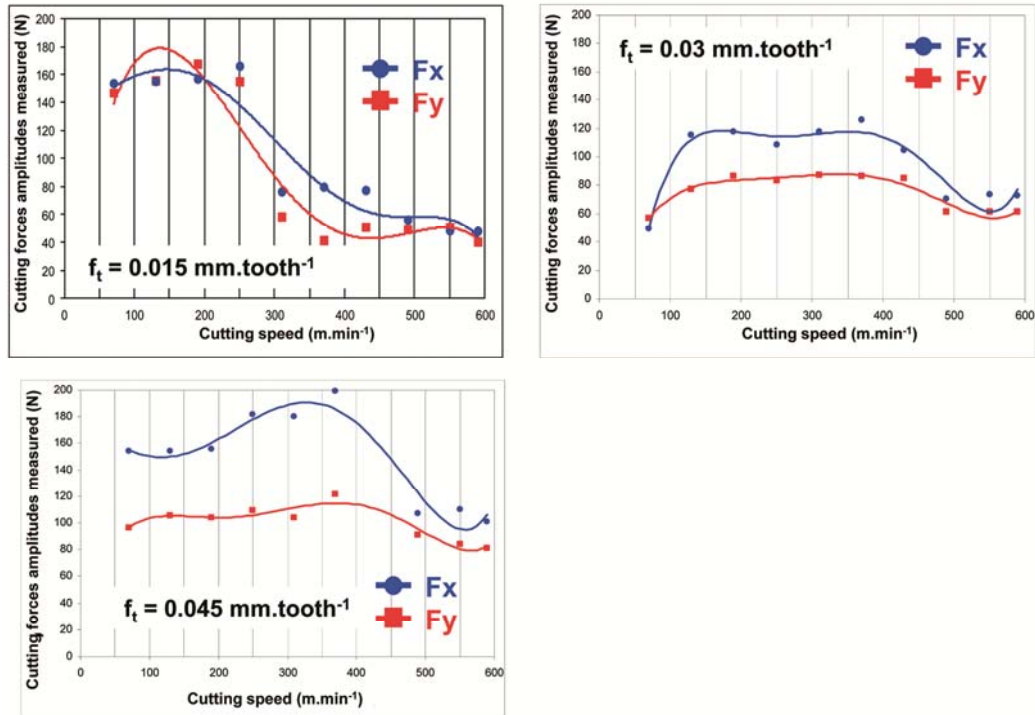


Fig.13. Cutting forces average amplitude evolutions function of cutting speed in down cutting configuration for end mills B.

- In return, on up cutting curves, the feed force F_y is greater than the transverse force F_x in critical zone. The transverse forces are theoretically upper than the feed forces in end milling for slotting configuration. It is commonly still the case for semi or even quarter immersion configuration [32]. Only inferior radial immersion can produce an inverse repartition, especially in up-cutting mode. This tendency to inverse the cutting forces repartition in up-cutting is due to two major phenomena: cutting efficiency of the cutting edge due to its sharpness in regard of the underformed chip thickness; and cutting stability due to dynamic tool's behaviour linked to its stiffness. In fact, the cutting force generated at the beginning of a new chip (see figure 7) is amplified when the sharpness of the tool is reduced (i.e. the cutting edge radius/chip thickness ratio becomes unfavourable), and during the whole tooth path in the part's material, the radial

component of the generated force tends to grow and the tangential one tends to decrease. These local modifications of cutting force amplitude and direction can change the repartition in force value between feed direction and transverse direction in milling. This observation is particularly evident in micro-milling where the sharpness of the tool is critical [35]. The previous results in up-cutting mode (figures 11 & 12) show that mill B tends to present this behaviour and not the mill A, it can be explained by the difference in tungsten carbide structure between these two uncoated mills. The micro grain tungsten carbide structure of the mill A gives to the tool a better sharpness and a better stiffness, that generate less cutting force amplitude and a repartition on reference axes closer to the theoretical rigid and perfectly sharp case, especially for intermediary cutting speeds (critical zone).

To conclude, three zones seem clearly appear from the experiments: two favourable machining zones and one unfavourable machining zone. Machining zones with stable machining conditions and with reduced cutting forces are described by a conventional machining zone between 0 and 200 $\text{m}\cdot\text{min}^{-1}$ and a high speed machining zones beginning from 550 $\text{m}\cdot\text{min}^{-1}$. The critical zone with severe cutting forces is described by a dead zone between 200 and 500 $\text{m}\cdot\text{min}^{-1}$. Many phenomena have to be noted. Firstly, in up cutting configuration with the bull nose end mills B the dead zone is wider than for the end mills A. And in down cutting configuration with the bull nose end mills B the dead zone does not exist. Nevertheless the high speed machining zone is observed on all the experimental results.

4.3 The tool run-out in milling

The tool run-out is a very important phenomenon in milling with strong influences on the tool engagement in matter. Indeed, the tool run-out modifies the theoretical position of mill cutting edges during machining. In this way, it is an important factor of cutting instabilities and tool wear. It particularly modifies the cutting edges loading repartition and then unbalances cutting forces and wear between the teeth. The tool run-out can be defined as a position gap between the spindle revolution axis and the tool axis as related in Figure 14. Classically, this phenomenon is divided in two different reference defaults:

- The axial tool run-out (angular gap between the tool axis and the spindle axis)
- The radial tool run-out (eccentricity of the tool axis in relation to the spindle revolution axis)

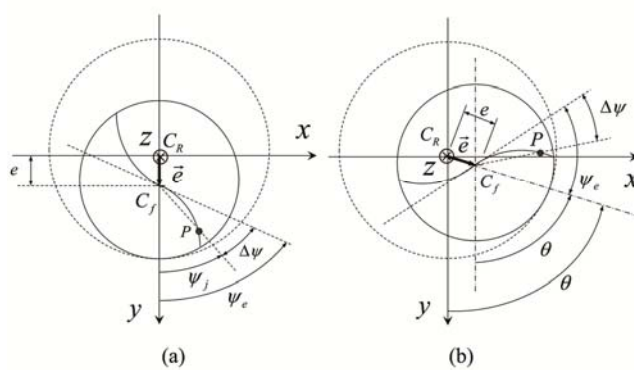


Fig.14. Parametric description of the tool run-out. (Fontaine et al., 2007)[12]

This default depends mainly on the qualities of spindle, tool holder and tool used. It has to be considered as one of the most severe defaults in machining and particularly in high speed machining. Its effects are critical in milling and dramatic in high speed milling or in micro milling because of the higher rotation frequencies used. The defects resulting to a critical run-out are form errors, amplified roughness, cutting instability, accelerated tool wear and breakage and

accelerated wear of the spindle bearings. The radial run-out is most of the time more pronounced and more difficult to compensate dynamically by the flexibility of the cutting system (tool + tool-holder) than the axial run-out. For example, modelling the radial run-out only usually permits to predict accurately the cutting forces unbalance [12][32][36]. That is the reason why we focus specifically on the radial defect in the following works.

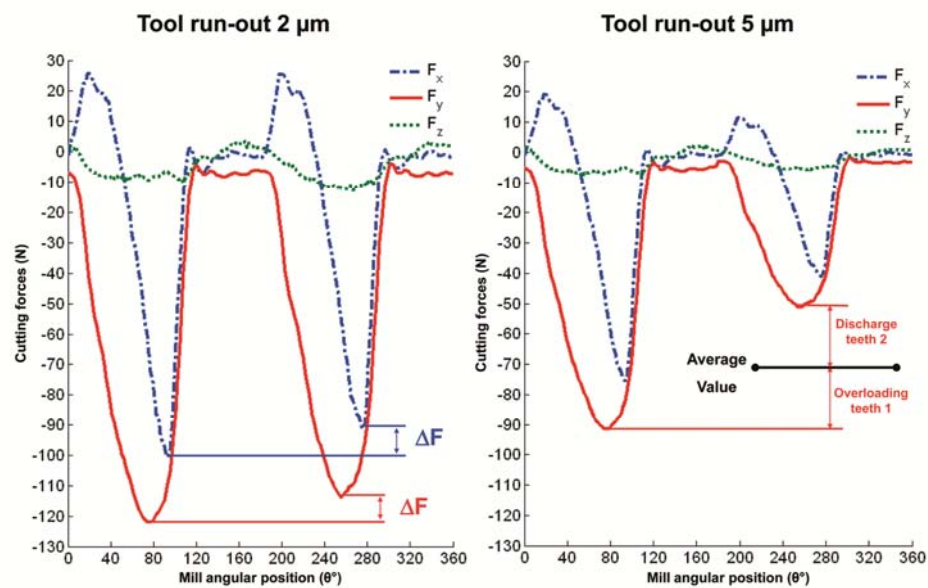


Fig.15. Influence of the tool run-out on cutting forces in milling

For the experiments led on with the uncoated end mills A, a measure of the tool run-out has been performed before each milling operation in order to quantify the values of the radial defect and to observe its influence on cutting forces in function of cutting speeds. Measurement has been performed with a charge amplifier and two position sensors fixed on the machine table and touching the cylindrical part of the tool along X and Y axis respectively. The maximal accuracy reached with this device is about 0.1 μm and the measures are really repeatable. The measurement protocol consists to slowly spin manually the mill in order to quantify the defect between the extreme positions which corresponds to

two times the value of eccentricity. The setting up is related in Figure 3. The tool run-out is here located by an eccentricity value e and an angular position of the maximal defect on the tool cylinder, like on the sketch related in Figure 14. For all the experimental tests in milling, the measured tool run-out took values between 2 μm and 5 μm .

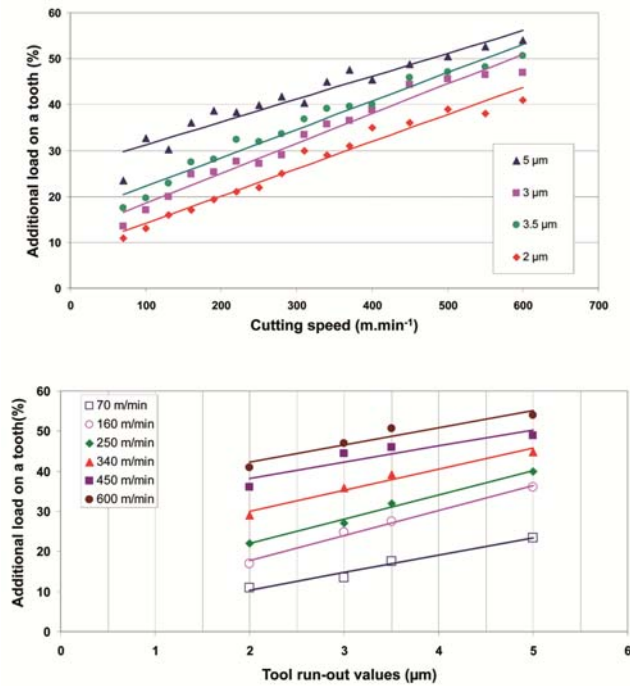


Fig .16. Additional loading evolution function of tool run-out and cutting speed

In case of conventional milling, this defect represents at maximum 30 % of tested feed per tooth. The tool run-out is not critical in milling but possesses a real influence on cutting stability, dynamics phenomena and tool wear. The tool run-out effect is described with two cutting forces curves and measured with two different tool run-out values, Figure 15. Each curves represents a mill rotation or in this case two tooth paths. On these curves, the tool run-out modifies the cutting forces repartition between each tooth of the mill. The additional loading on a tooth is a proposed value to quantify tool run-out effect. This value is a percentage of the cutting forces average value. It is added positively or negatively on each tooth. So with this definition, overloading and discharge are equal and opposite, and

during our experiments the maximal value of measured overloading exceeds 50 % of the average cutting forces. After experimental analysis, the behaviour of this additional loading has been observed in function of tool run-out values and cutting speeds, and the results are related in Figure 16. On these curves, additional loading increases in an important way with cutting speed, then the tool run-out effect seems to increase with cutting speed. Moreover the additional loading increases linearly with the tool run-out values and increases globally with cutting speed. For high cutting speeds and due to dynamic effects, the tool run-out phenomenon can become a critical point for tool behaviour, machined surface quality and tool wear.

4.4 Chip formation

Chips give essential information about milling process. They are the results of the matter deformation and also the witness zone of the most intense mechanical or thermal solicitations occurring in cutting. In literature, a very few works focused on chip observations in up cutting configuration in milling. That is right that it is very difficult to make a connection between the chip geometry and its way of formation, because the final shape of a chip can be very different from the theoretical shape which can be deduced from a rigid and elementary case. In turning, this difference is reduced, so it is easier to conclude. In this analysis, the aim not consists to compare a real chip with a chip in a theoretical case, but rather to observe differences and evolutions in chip morphology in function of machining parameters. A first qualitative analysis is here proposed, and then completed in analysing the evolutions of chip length and thickness.

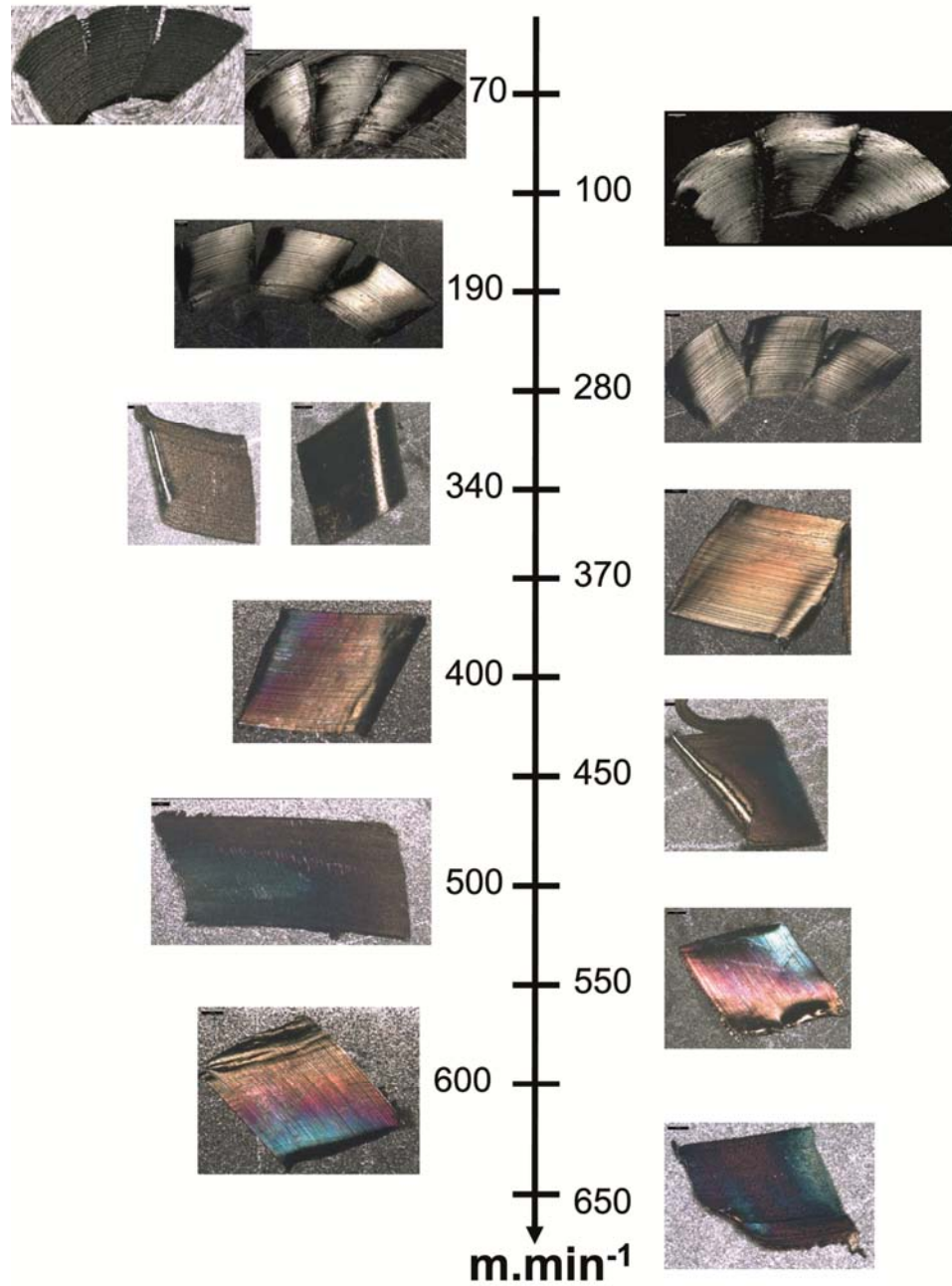


Fig .17. Chip evolution function of cutting speed in milling of a 304L steel

The qualitative analysis related in Figure 17 shows that the obtained chips inherit some characteristics of the mill flute, and in particular a striated surface due to the ploughing of the chip by irregularities of the rake face of the flutes obtained after tool grinding. The metallic aspect of chips is close to the initial material but for a cutting speed equal to $450 \text{ m}\cdot\text{min}^{-1}$, an important changing appears on the chip surface. Oxide colours (red, blue, orange) appeared on chip surface, it is probably due to the thermal effects induced by high cutting and friction speeds.

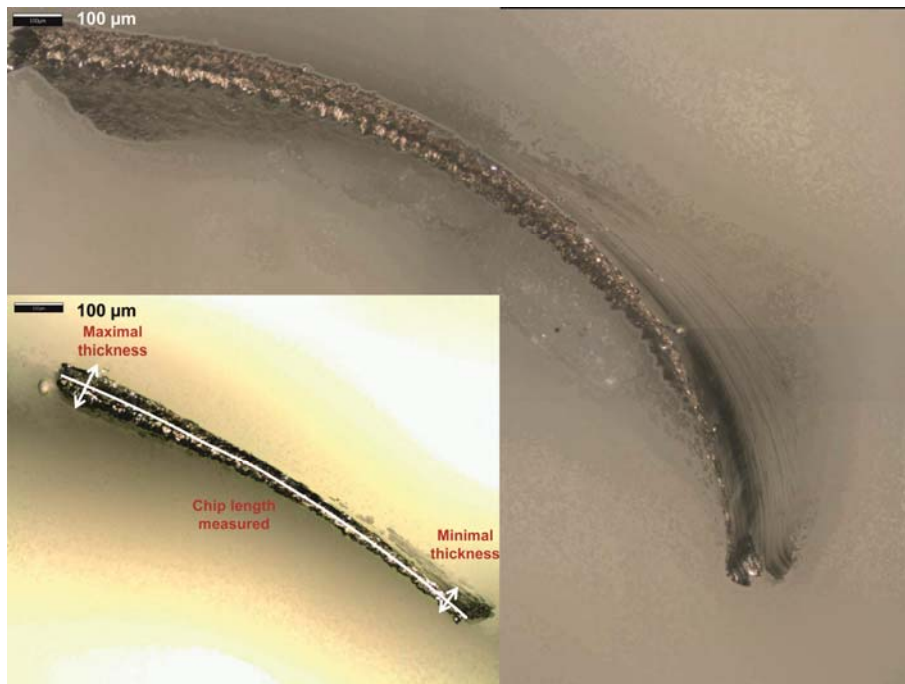


Fig .18. Characteristic shape of a chip obtained after semi-immersion milling tests.

A quantitative analysis has been performed with measurements of chip length and thickness with a topo-microscope as related in Figure 18. The chip length is measured in taking into account the 3D curve shape, and we choosed to determine length with the best curve passing along the chip. Concerning, the chip thickness, we measured the maximal and the minimal thickness in orthogonal direction of the curve chip. Each measurement are based on 5 same cutting condition chips, then the average maximal and minimal thickness is calculated, and the global average thickness is deduced. Results are related in Figure 19 and the following observations have been made:

- Firstly, the chip length is always smaller than the theoretical length which can be deduced from a rigid case as related in Figure 5, Figure 7 and Figure 9.
- Secondly, on all curves, the same tendency is observed, the chip length decreases with the increase of the cutting speed and three stages appear : a

first zone of fast decrease followed by two stationary zones. The stages cutting speed limit values are different in function of the feed, but the discrepancy is relatively small.

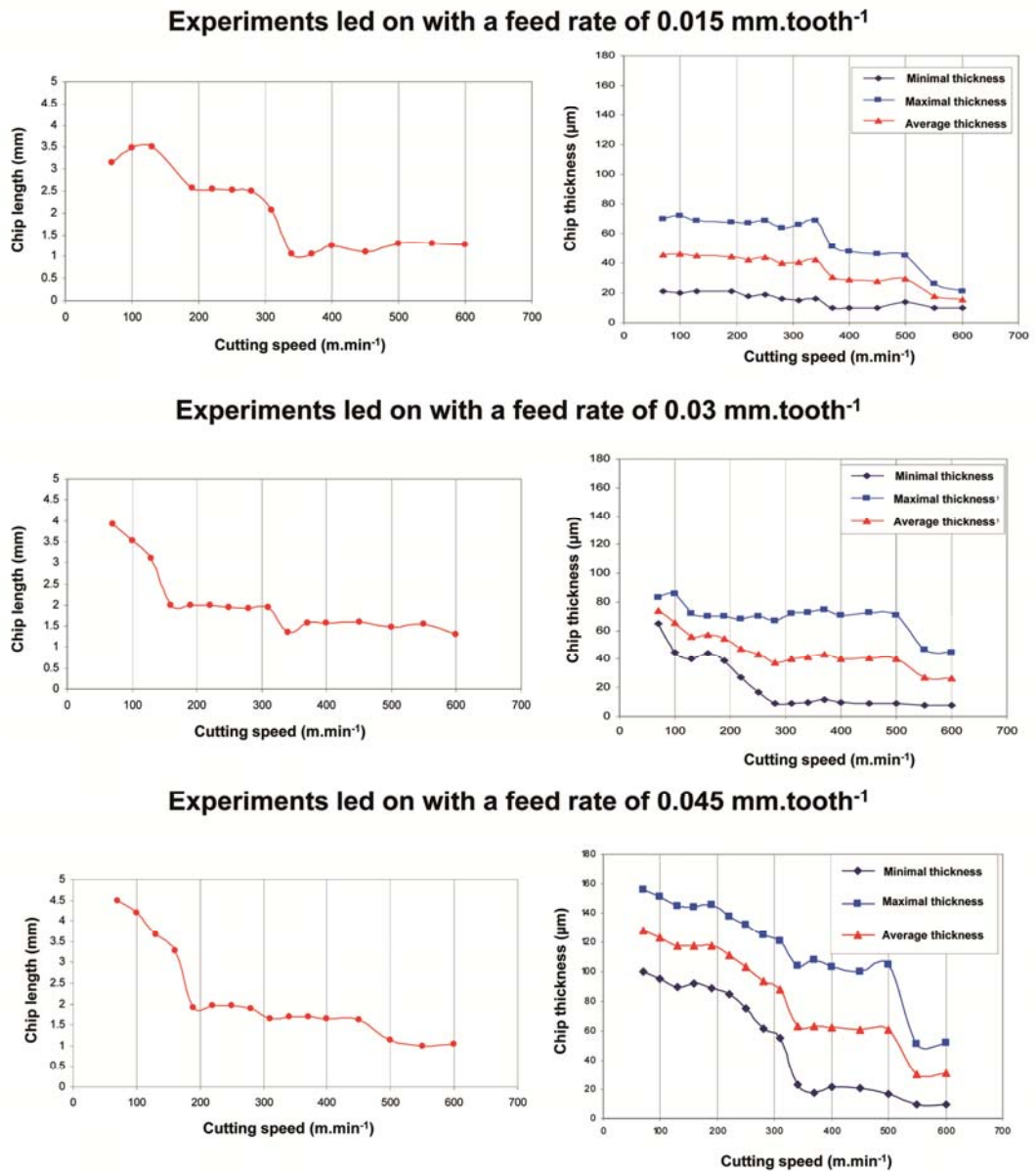


Fig .19. Evolution of chip thickness and length function of cutting speed for three values of feed.

- About the chip thickness, for each feed, three curves are related in Figure 19. Because the chips have commonly a characteristic shape as related in Figure 18, minimal and maximal thicknesses have to be measured. Indeed, in a shoulder milling test in up cutting configuration, the tool engagement

begin with a chip thickness close to 0 mm and finish with a theoretical chip thickness equal to f_t (Figure 7). The real geometry is very far of the rigid case, because the shearing due to the cutting process induces a lot of compression in length direction and of spreading in thickness direction. The average thickness has been calculated and added to describe the evolution in global way. On these curves, the same behaviour than for the chip length is observed: a first zone of decrease followed by two stationary zones.

It is easy to compare these results with the results obtained on machinability curves. In both cases, three stages are observed with the same limit in terms of cutting speed values. Moreover this analysis put in evidence a high cutting speed zone where the chip formation seems to be characterized by low chip length and thickness and then a high material compression occurring during chip formation. To conclude, the milling process implies a favourable high speed machining zone which is characterised by lower cutting forces and a different way of chip formation. It corresponds to remarks often made in literature but it deserves to be shown experimentally for milling [37][38].

4.5 Mill geometry evolution

On all the experiments, the wear of mills has been analysed in a qualitative way by comparing the mill after the test with a new one, It was chosen in this section to relate the measurements for the mills A in Figure 20 and Figure 21 for a cutting speed of $500 \text{ m}\cdot\text{min}^{-1}$ and different feed rates. All observations have been performed with the topo-microscope Alicona.

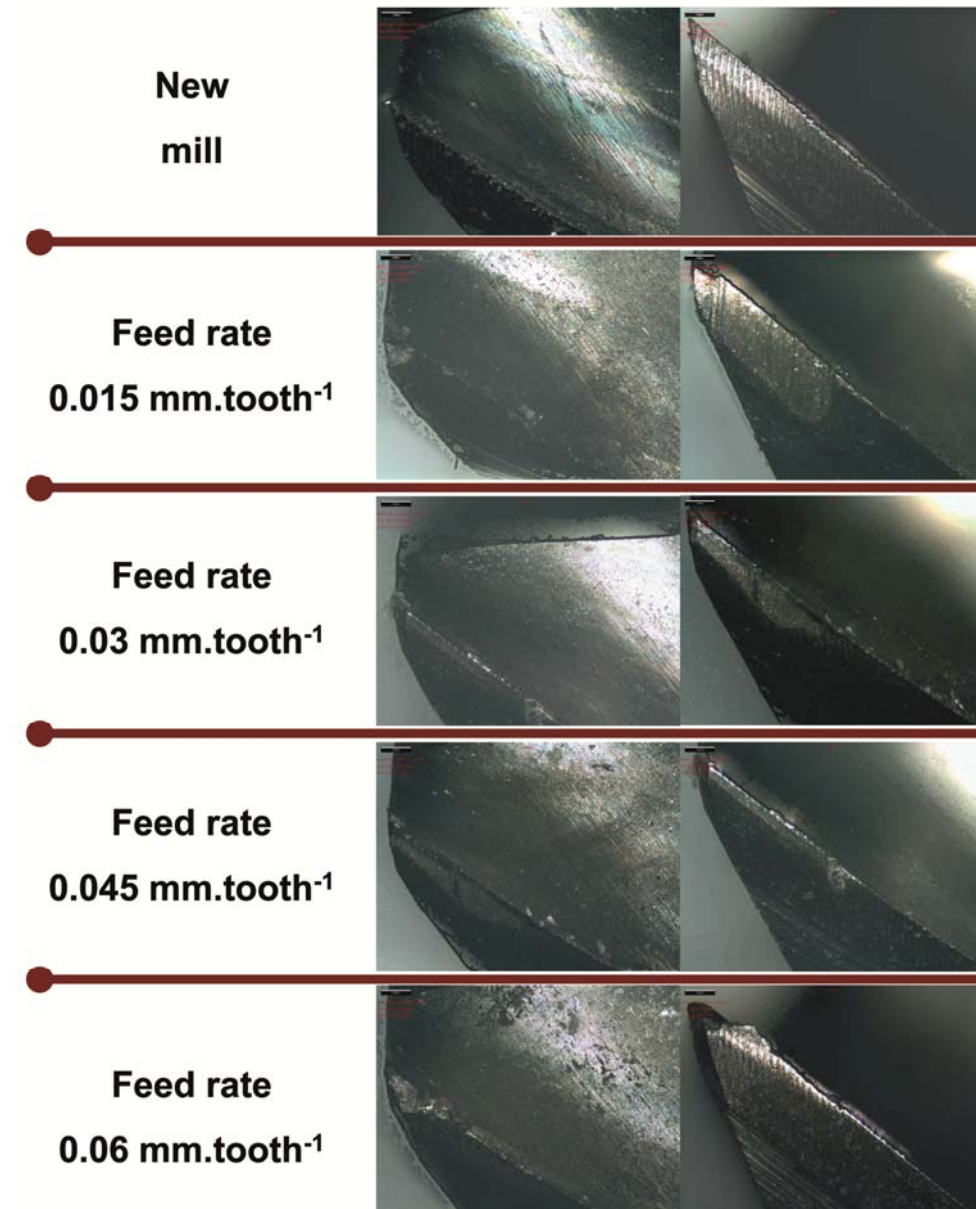


Fig .20. Characteristic wear of mills for different feed rates.

The results are related in Figure 20 and the following conclusions can be done:

- For low feed rates, an important abrasive wear is observed on the relief face of the mill.
- For higher feeds, abrasive wear is reduced but a radius tends to appear at the extremity of the end mills A for high cutting speeds. Moreover, the relief face presents an irregular wear with cracks and craters.

- For the highest feed (i.e $0.06 \text{ mm.tooth}^{-1}$) and moderate cutting speeds, some teeth of end mills broke suddenly.
- For high cutting speeds, the coating of mills is usually fast deteriorated (abrasion and delamination).

For these experiments which induce a short machining time, the rake faces and mill flutes do not showed a real wear. Indeed, for high cutting speeds, the decrease of chip length tends to limit the contact between chips and mill flutes or rake faces. In these cutting conditions, the chip seems to be ejected. That's why during our experiments, we have observed unidirectional chip flows with a regular rate from 500 m.min^{-1} . Then, a more accurate analysis has been performed on mills used for two different feeds and on a new mill for a set of experiments from 70 m.min^{-1} to 650 m.min^{-1} . With the topo-microscope Alicona, the teeth of each tool have been rebuilded in three dimensions, in order to quantify the wear phenomena and to focus on the evolution of cutting edges geometry. Measures of tool edge sharpness at different level on tool axis have been carried out with the optical 3D InfiniteFocus© measurement device. Figure 21 (a), (b) and (c) describe respectively results obtained with a new mill, mills used with a feed of $0.015 \text{ mm.tooth}^{-1}$ and with mills used with a feed of $0.03 \text{ mm.tooth}^{-1}$. The optical pictures of mills are proposed to locate the measurement sections along the cutting edges. The local profiles are shown to put in evidence the real shape of cutting edges in different places. The following results have been obtained:

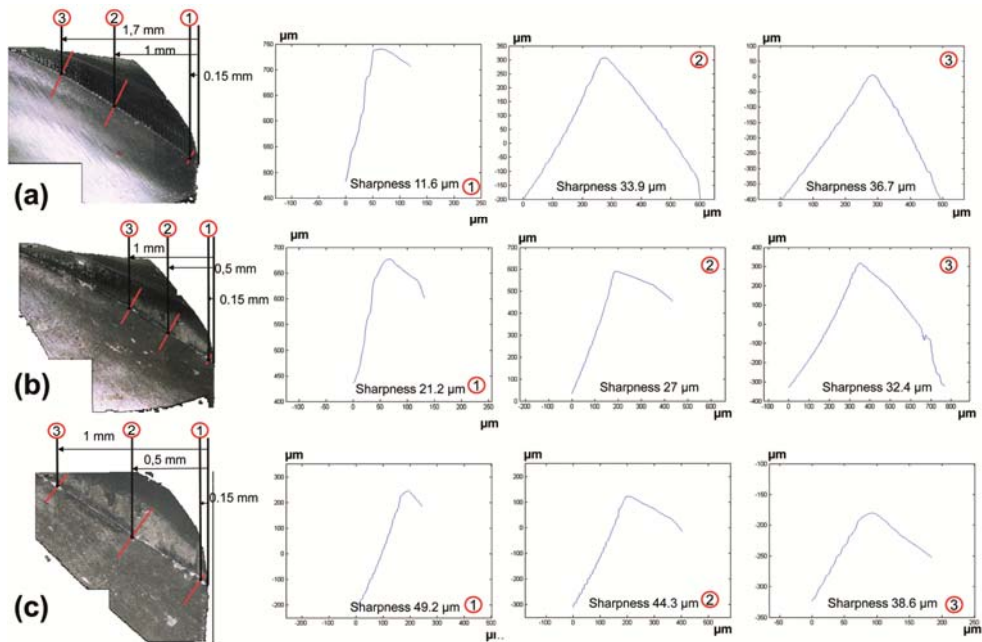


Fig .21. Evolution of cutting edges sharpness for different feed rates.

- The new mill is exposed in Figure 21 (a). Different pictures allow verifying the tool geometry, measuring sharpness and observing the path of diamond grinding wheel due to the tool manufacturing process. The perfect reliability of cutting edge is put in evidence. On the other hand, sharpness of cutting edge has shown interesting results. Three measurement zones are appeared during analysis. The mill, between a height of 0 mm and 0.5 mm along the tool axis, has a cutting edge sharpness equal approximately to 12 μm . Then between a height of 0.5 mm and 1 mm, a linear evolution of sharpness is observed between the two values 12 μm and 34 μm . For a height superior to 1 mm the sharpness has a constant value equal approximately to 39 μm . So, the sharpness is low on a small zone of the tool and becomes quickly higher. The cutting edge is far away of the perfect sharpness classically used in analytical models. But these measures are very useful for finite element modelling, because for a suitable monitoring of the contact mechanisms, the perfect

sharp edges are very harmful. Introduction of this radius in tool mesh is very important to perform milling process simulations [20].

- Results obtained with mills used for milling operation with a feed of 0.015 mm.tooth-1 are related in Figure 21 (b). The picture put in evidence the abrasive wear on the relief face of the tool. The sharpness measures have been led on the cutting edge zone engaged in matter (height between 0 mm and 1 mm along tool axis). Results indicate that the wear at the tool extremity is very important. In this zone, mill has lost 10 μm of sharpness. In the other hand, low feeds seem to create less wear in height between 0.5 mm and 1 mm where sharpness is about 27 μm in low zone and 32 μm in high zone. Moreover low feeds seem to create a very important abrasive wear on the relief face of the tool. The influence of high cutting speed appeared only on abrasive wear of the relief face in this case.
- Results obtained with mills used for milling operations with a feed of 0.03 mm.tooth-1 are related in Figure 21 (c). Measurements show a severe wear of the cutting edge. The wear seems to be more critical due to the high value of feed particularly when high cutting speeds are reached. At the extremity of the tool, sharpness of 49 μm has been measured and in this zone the cutting edge is chamfered by wear.
- Some cracks and craters are generated during machining on the relief face at tool extremity and this phenomenon becomes very important for high cutting speeds. Then cutting edge has a sharpness of 45 μm , but at a height near to 1 mm the value is about 38 μm and in this zone the wear seems to be still restrained. From these measurements no significant wear is observed on the rake face of the tool, even for high cutting speeds.

These analyses put in evidence different wear phenomena and allow quantifying the quick reduction of the cutting edges sharpness in many feeds and for the high speed machining zone. Results have shown that dominant wear phenomena depend to feeds and cutting speeds values. These investigations can provide a relevant sharpness value to finite element or analytical model developers.

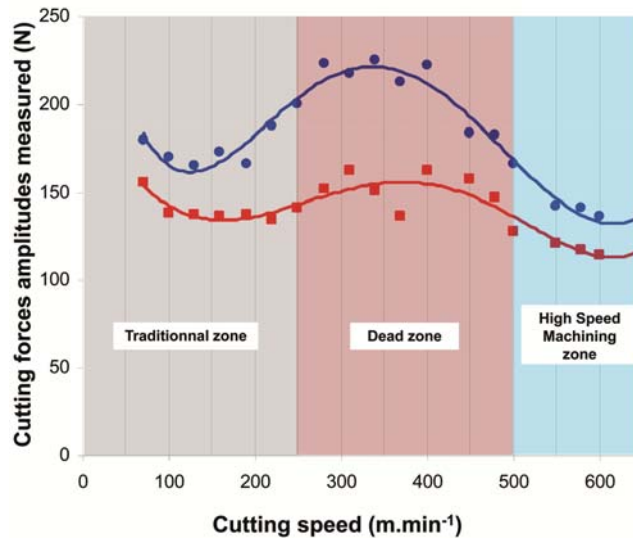


Fig .22. Representative machinability of the tested 304L stainless steel in milling (feed rate 0.045 mm.tooth⁻¹, end mill A 2 teeth micro grain tungsten carbide, diameter 6 mm, d_a 1 mm, d_r 3 mm) .

5 Conclusions

These works furnish a wide experimental basis in milling and high speed milling of a 304L stainless steel. These data are proposed to help engineers and researchers to understand the milling process specificities and key points, but also to develop or to improve modelling of machining. A wide range of experiments has been performed with a large panel of cutting conditions, tool geometries or cutting configurations in slotting and shouldering. The set up acquisition system allows obtaining a good accuracy and repeatability on cutting forces curves. These milling curves are used as main data to analyse the cutting edges engagement in machined material, the appearing of dynamic effects with the increase of cutting speed, the influence of tool run-out and to identify proper cutting conditions in

terms of cutting speed and feed rate. These results were also used for our parallel works on numerical simulation [20] or identification [31]. The cutting forces data are completed with information about chips morphology and tools wear.

The experiments led on with mills A and B for different cutting speeds and feeds have furnished a very important experimental database, and all available data has been analysed in order to put in evidence the physical phenomena induced by milling operations. The analysis of cutting forces curves for many cutting speeds has shown that dynamic phenomena appear during machining particularly in shoulder milling configuration. With these dynamic effects, the measured cutting forces curves are far away from the curves obtained analytically in a rigid case or for low cutting speeds. Until now modelling of milling from analytical or finite element models used the assumption of undeformable tools. But this assumption limits drastically the model predictivity until the low conventional cutting speeds are overpassed. The machinability of the 304L stainless steel with different tools geometries and configurations in shoulder milling is defined by three working zones: a conventional zone permitting stable cutting (low cutting speed; under $200\text{-}250\text{ m}\cdot\text{min}^{-1}$), a dead zone (unfavourable for cutting forces level and cutting stability; between 250 and $450\text{ m}\cdot\text{min}^{-1}$), and a high speed machining zone (high cutting speed; up to $450\text{-}500\text{ m}\cdot\text{min}^{-1}$). All the used criteria (cutting forces, chips, wear) confirm the existence of these different zones and a correlation is proposed with cutting perturbations as run-out, cutting instability, ploughing and abrasive wear.

Then the tool run-out influence has been described and measured for many experiments. With increase of cutting speed, tool run-out accentuates vibrations and unbalances cutting forces repartition and wear between the teeth. The analysis led on tool wear has permitted to set up a methodology to measure cutting edges

sharpness on mills in order to introduce a real description of the tool geometry in finite element or analytical modelling. All these conclusions are useful to improve models predictivity and to extend modelling to high speed machining zone. These results confirm the assumption of the changing of thermo-mechanical conditions from the cutting speed equal approximately to $450 \text{ m}\cdot\text{min}^{-1}$. It underlines the difficulty to choose and identify a constitutive law to describe the material behaviour, because high strain rate and high temperatures corresponding to the high speed zone are non accessible with classic mechanical tests.

In this context, the choice of cutting coefficients or laws used to model empirically the milling process needs to consider a tight panel of cutting conditions to stay representative. In the same way predictive modelling of machining needs to use constitutive laws to describe material behaviour and friction conditions, so the huge variations in the process response are a limitation. For example, in our modelling works a Johnson & Cook constitutive law was tested and permitted to obtain very good results in the first zone (low to medium cutting speeds). In the other working zones, this law is not really efficient, especially when the strain rate and temperature influences for our stainless steel are identified on classical mechanical test. We have the same considerations when friction is considered through a constant coefficient. So it is necessary to find an appropriate constitutive law relevant on a wide range of thermo-mechanical solicitations. In the same way, the friction conditions and their modelling at the tool chip interface have to be analysed further. Moreover classical mechanical characterisation tests are inefficient for extreme strain rates coupling to high temperatures. As a first step, the development of constitutive laws and identification by inverse method using measured data obtained directly from milling tests (as cutting forces curves) seems to be an interesting way to improve

milling models as demonstrated in previous work (Maurel-Pantel et al., 2008) [31]. In analytical or finite element models developed by our team and using rigid tool assumption have shown their limits to reproduce the cutting forces curves measured at high cutting speeds. In machining models actually, the dynamics and thermo-mechanical coupling introduced by high cutting speed are not taken into account. These detailed experimental data in milling constitute a suitable experimental basis available to develop predictive machining modelling. Now the characterisation of cutting dynamics become a major experimental challenge in high speed milling or in micro milling. And It becomes also a challenge in modelling to develop predictive analytical of finite element models at high cutting speeds in milling.

Acknowledgements

The CETIM foundation is greatly acknowledged for providing the PhD grant support to Dr A. Maurel-Pantel in the PGV project. These works were carried out in the context of the working group Manufacturing 21 which including 18 French laboratories. Targeted issues are the modelling and the optimization of manufacturing processes and the innovation in the field of mechanical manufacturing. Thanks to F. Gaillard from DIAGER Industry® for his help in choosing and obtaining tools.

References

1. Merchant M (1945) Mechanics of the metal cutting process, i. orthogonal cutting, *Journal of Applied Physics* 16:267-275.
2. Oxley P (1963) Mechanics of metal cutting. *ASME* 50-60.
3. Ceretti E, Fallbohmer P, Wu W, Altan T (1996) Application of 2D FEM to chip formation in orthogonal cutting. *Journals of Materials Processing Technology* 59:169-180.
4. Baker M (2005) Finite element investigation of the flow stress dependence of chip formation. *Journals of Materials Processing Technology* 167:1-13.
5. Kline WA, DeVor RE, Lindberg JR (1982) The prediction of cutting forces in end milling with application to cornering cuts. *International Journal of Machine Tool Design and Research* 22-1:7-22.
6. Yellowley I (1985) Observations of the mean values of forces, torque and specific power in peripheral milling process. *International Journal of Machine Tool Design and Research* 25(4):337-346
7. Yang M, Park H (1991) The prediction of cutting force in ball-end milling. *International Journal of Machine Tools and Manufacture* 31(1):45-54.

8. Altintas Y, Lee P (1996) A general mechanics and dynamics model for helical end mills. *CIRP Annals – Manufacturing Technology* 1: 59-64
9. Engin S, Altintas Y (2001) Mechanics and dynamics of general milling cutters. Part I: helical end mills. *International Journal of Machine Tools and Manufacture* 44:2195-2212.
10. Engin S, Altintas Y (2001) Mechanics and dynamics of general milling cutters. Part II: inserted cutters. *International Journal of Machine Tools and Manufacture* 41:2213-2231.
11. Zhu R, Kapoor SG, DeVor RE (2001) Mechanistic modelling of the ball end milling process for multi-axis machining of free-form surfaces. *Transactions of ASME, Journal of Manufacturing Science and Engineering* 123:369-379.
12. Fontaine M, Devillez A, Moufki A, Dudzinski D (2006) Predictive force model for ball end milling and experimental validation with a wavelike form machining test. *International Journal of Machine Tools and Manufacture* 46:367-380.
13. Molinari A, Dudzinski D (1992) Stationary shear band in high speed machining. *C.R. Académie des Sciences de Paris* 315:399-405.
14. Dudzinski D, Molinari A (1997) A modelling of cutting for viscoplastic materials. *International Journal of Mechanical Science* 39:369-389.
15. Moufki A, Devillez A, Dudzinski D, Molinari A (2004) Thermomechanical modelling of oblique cutting and experimental validation. *International Journal of Machine Tools & Manufacture* 44(9):971-989.
16. Zeroudi N, Fontaine M, Necib K (2010) Prediction of cutting forces in 3-axes milling of sculptured surfaces directly from CAM tool path. *Journal of Intelligent Manufacturing*, 15:1-15.
17. Zeroudi N, Fontaine M (2012) Prediction of machined surface geometry based on analytical modelling of ball-end milling. *Procedia CIRP* 1:108-113.
18. Shao H, Liu L, Qu HL (2007) Machinability study on 3%Co-12%Cr stainless steel in milling. *Wear* 263:736-744.
19. D'Errico GE, Bugliosi S, Guglielmi E (1998) Tool-life reliability of cermet inserts in milling tests. *International Journal of Materials Processing Technology* 77:337-343.
20. Maurel-Pantel A, Fontaine M, Thibaud S, Gelin JC (2012). 3D FEM simulations of shoulder milling operations on a 304L stainless steel. *Simulation Modelling Practice and Theory* 22:13-27.
21. Tekiner Z, Yesilyurt S (2004) Investigation of the cutting parameters depending on process sound during turning of AISI 304 austenitic stainless steel. *Materials and Design* 25:507-513.
22. O'Sullivan D, Cotterell M (2002) Machinability of austenitic stainless steel SS303. *International Journal of Materials Processing Technology* 124:153-159.
23. Salak A, Vasilko K, Selecka M, Danninger H (2006) New short time face turning method for testing the machinability of PM steels. *International Journal of Materials Processing Technology* 176:62-69.
24. Senthil Kumar A, Raja Durai A, Sornakumar T (2006) The effect of tool wear on tool life of alumina-based ceramic cutting tools while machining hardened martensitic stainless steel. *International Journal of Materials Processing Technology* 173:151-156.
25. Akasawa T, Sakurai H, Nakamura M, Tanaka T, Takano K (2003) Effects of free cutting additives on the machinability of austenitic stainless steels. *International Journal of Materials Processing Technology* 143-144:66-71.

26. Valiorgue F, Rech J, Hamdi H, Bonnet C, Gilles P, Bergheau JM (2008) Modelling of friction phenomena in material removal processes. *International Journal of Materials Processing Technology* 201:450-453.
27. Valiorgue F, Rech J, Hamdi H, Gilles P, Bergheau JM (2012) 3D modeling of residual stresses induced in finish turning of an AISI304L stainless steel, *International Journal of Materials Processing Technology* 53:77-90.
28. Bonnet C, Valiorgue F, Rech J, Claudin C, Hamdi H, Bergheau JM, Gilles P (2008) Identification of a friction model-Application to the context of dry cutting of an AISI 316L austenetic stainless steel with a TiN coated carbide tool. *International Journal of Machine Tools and Manufacture* 48:1211-1223.
29. Johnson GR, Cook JR (1983) Constitutive model and data for metals subjected to large strains, high strain rates, and high temperatures. *Proceedings of 7th Symposium On Ballistics, Netherlands*.
30. Maurel-Pantel A, Michel G, Thibaud S, Fontaine M, Gelin JC (2008) 3D FEM simulations of milling on a 304L stainless steel. *Steel Research International* 79(2):726-733.
31. Maurel A, Fontaine M, Thibaud S, Michel G, Gelin, JC (2008) Inverse Method for Identification of Material Parameters Directly from Milling Experiments. *International Journal of Material Forming* 1:1435-1438.
32. Fontaine M, Devillez A, Dudzinski D (2007) Parametric geometry for modelling of milling operations. *International Journal of Machining and Machinability of Materials* 2:186-205.
33. More AS, Jiang W, Brown WD, Malshe AP (2006) Tool wear and machining performance of cBN-TiN coated carbide inserts and PCBN compact inserts in turning AISI 4340 hardened steel *Journal of Materials Processing Technology* 180(1-3):253-262.
34. Chandrasekaran H, Johansson JO (1994) Chip Flow and Notch Wear Mechanisms during the Machining of High Austenitic Stainless Steels *CIRP Annals - Manufacturing Technology Volume* 43(1):101-105.
35. Gilbin A, Fontaine M, Michel G, Thibaud S, Picard P (2013) Capability of tungsten carbide micro-mills to machine hardened tool steel *International Journal of Precision Engineering and Manufacturing* 14(1):23-28.
36. Fontaine M, Moufki A, Devillez A, Dudzinski D (2007) Modelling of cutting forces in ball-end milling with tool-surface inclination. Part II: Influence of cutting conditions, run-out, ploughing and inclination angle. *Journal of Materials Processing Technology* 189:85-96.
37. Abukhshim NA, Mativenga PT, Sheikh MA (2006) Heat generation and temperature prediction in metal cutting: A review and implications for high speed machining *International Journal of Machine Tools and Manufacture* 46(7-8):782-800
38. Abou-El-Hossein KA, Yahya Z (2005) High-speed end-milling of AISI 304 stainless steels using new geometrically developed carbide inserts *Journal of Materials Processing Technology* 162-163:596-602.